RSC Mechanochemistry

ROYAL SOCIETY OF CHEMISTRY

PAPER

View Article Online
View Journal | View Issue

Cite this: *RSC Mechanochem.*, 2024, **1**, 465

Ball milling assisted mechano-catalytic dye degradation using $SrTiO_3$ nanoparticles†

Aman Shukla,[ab] Akshay Gaur,[a] Shivam Dubey[a] and Rahul Vaish *[a]

Ball milling stands as a versatile and widely used technique that involves the mechanical grinding of solid materials *via* ball mills. Conventionally employed for synthesizing nanomaterials and complex compounds, this method has now been harnessed directly for catalysis due to its capability for surface charge separation. Herein, in the present study, we have explored the potential of ball milling to activate material with low piezoelectric coefficient for catalysis by demonstrating the ball-milling-induced mechano-catalytic activity of $SrTiO_3$ (STO) nanoparticles for the degradation of toxic methylene blue (MB) dye. With the assistance of ball milling, STO nanoparticles (of 0.3 g dosage) were found capable of degrading 70% of 10 ppm MB dye at 400 rpm speed with 10 Zr balls in just 1 hour. A series of parametric studies were performed to analyze the effect of various process conditions, like catalyst dosage, initial concentration of dye, ball milling speed, and number of milling balls. Further, scavenging tests were carried out to detect the responsible reactive species for dye degradation. Moreover, the present ball milling process was compared with the trivial ultrasonication method where STO showed just 12% degradation in 1 hour. The results manifest the superiority of ball milling catalysis which not only offers precise control over reaction parameters but also encompasses scalability, simplicity, and better potential to conduct catalysis under environmentally benign conditions.

Received 8th May 2024
Accepted 9th August 2024

DOI: 10.1039/d4mr00047a

rsc.li/RSCMechanochem

1. Introduction

Global challenges persist in the form of water scarcity and contamination, impacting communities worldwide and posing substantial threats to public health and the environment. The escalating environmental concern involves water pollution induced by hazardous organic dyes, commonly utilized in industries like textiles, leather processing, and printing.[1–3] Improper disposal practices allow these dyes to enter water bodies, posing risks due to their persistence and potential toxicity. The discharge of organic dyes into rivers or lakes can lead to changes in water colour, reduced light penetration, and disruption of aquatic life by inhibiting photosynthesis.[4] Some dyes may get converted into harmful by-products, further compromising water quality.[5] Researchers are actively exploring innovative materials and methodologies to develop sustainable water purification technologies. Activated carbon adsorption, a prevalent method, involves porous carbon particles attracting and trapping organic dyes.[6] However, challenges include potential saturation and, necessitating frequent replacement. Biological treatment, utilizing microorganisms, is eco-friendly but may have limitations in degrading certain dyes with milder efficiency.[7] Membrane filtration, such as reverse osmosis, effectively removes dye particles but requires substantial energy inputs and may generate brine waste.[8] Among these, advanced oxidation processes (AOPs) always remain at the forefront of innovative water purification strategies, owing to the generation of reactive oxygen species, holding promise to degrade emerging contaminants and improving the overall quality of water resources.[9,10]

Piezocatalysis represents an emerging frontier in the realm of advanced oxidation processes (AOPs), offering innovative avenues for water purification and pollutant degradation.[11,12] Unlike traditional AOPs that rely on chemical agents or external energy sources, piezocatalysis capitalizes on the unique ability of materials to convert mechanical energy into electrical energy, which can then activate catalysts to facilitate oxidation reactions. In piezo catalysis, the mechanical stress applied to piezoelectric materials induces charge separation, creating an electric field at the catalyst surface. This electric field promotes the generation of reactive oxygen species (ROS), such as hydroxyl radicals ($^{\cdot}OH$), which are highly effective in degrading organic pollutants and disinfecting water. Moreover, piezocatalysis offers several advantages over traditional AOPs. It operates under ambient conditions without the need for external energy sources, making it energy-efficient and environment friendly. However, the prerequisite for piezocatalysis process is non-centrosymmetric structure of the catalyst.

[a]*School of Mechanical & Materials Engineering, Indian Institute of Technology, Mandi, Himachal Pradesh, 175005, India. E-mail: rahul@iitmandi.ac.in*

[b]*Department of Material Science & Engineering, Indian Institute of Technology, Kanpur, Uttar Pradesh 208016, India*

† Electronic supplementary information (ESI) available. See DOI: https://doi.org/10.1039/d4mr00047a

Additionally, piezocatalysts can be easily integrated into existing water treatment systems, offering a scalable and cost-effective solution for addressing water pollution challenges. So far, piezoelectric materials like quartz, barium titanate, lead titanate, lead zirconium titanate, strontium titanate, lithium niobate, *etc.*, have been extensively studied for a wide variety of applications from hydrogen generation to water purification, from actuators to ultrasonic devices, from piezoelectric motors to underwater acoustics, *etc.*[13–19]

Regarding catalytic applications, these materials are utilized while subjected to ultrasonication. While piezocatalysis through ultrasonication can be effective in certain scenarios, such as enhancing mass transfer or breaking down aggregates, its application may be limited in terms of scalability and control over reaction parameters, which are crucial aspects of catalysis. Moreover, the intense cavitation process induced by ultrasound waves can also cause physical damage to the piezocatalyst material, reducing its lifespan and efficiency over time.[20] To address these issues, ball milling technique has emerged as a potential option to supply adequate mechanical energy required for piezocatalysis.

Ball milling stands as a versatile and widely used technique for refining precursors into powder form.[21] Additionally, ball milling is utilized in chemical synthesis, entailing the mechanical grinding of solid substances *via* ball mills.[22] This technique is traditionally employed for the synthesis of nanomaterials and complex compounds due to its ability to control reaction parameters such as milling time, speed, and the choice of milling media. In recent times, scientists have utilized the ball milling technique as a direct driver for catalysis due to its capability for surface charge separation.[23–27] This heightened surface charge separation, achieved through ball milling, offers a distinctive and potent mechanism for catalytic materials, enabling their effective involvement in various chemical transformations. During the high-energy ball milling process, solid materials experience intense mechanical forces and collisions with milling balls, leading to the generation of charge carriers on the surface of the particles.[28] This process induces a localized disruption of the crystal lattice, creating defects, vacancies, and reactive sites on the material's surface. The resulting electronic and structural changes contribute to the separation of charge carriers, with electrons and holes occupying different energy states. This charge separation phenomenon is particularly advantageous for catalytic applications, as it promotes efficient electron transfer and generation of reactive oxygen species. The advantages of ball milling include its scalability, simplicity, and the possibility of performing reactions under environmentally benign conditions.

Strontium titanate (STO), is one of the known materials for its exceptional qualities in various scientific and technological fields.[29,30] Its perovskite crystal structure contributes to its outstanding electronic, optical, and chemical properties. Notably, STO shows promise in environmental and energy applications due to its photocatalytic activity under UV light, aiding in environmental cleanup and solar energy conversion.[31] Moreover, its biocompatibility makes it suitable for biomedical uses like implants and drug delivery systems.[32–35] While pure cubic STO may not exhibit strong piezoelectric properties due to its centrosymmetric structure, piezoelectric effects can be induced under specific conditions such as strain-induced polarization or through defect introduction. Thus, achieving high piezocatalytic efficiency with pure STO remains a challenge, highlighting the need for further research to explore methods for maximizing its catalytic potential. Further, there are many cases in the literature, where the degradation of organic pollutant can be due to the surface charges generated on the catalyst when subjected to mechanical vibrations.

As per our limited knowledge, no study has been done so far to examine whether the piezo catalytic activity of materials with low piezoelectric coefficients like STO can be induced and enhanced by ball milling or not. Herein, we specifically chose STO despite its non-piezoelectric nature. The primary objective was to investigate whether the mechanical vibrations generated by the ball milling process can induce sufficient strain in STO, making it potentially useful for piezoelectric catalytic applications. The rationale behind this choice is rooted in the hypothesis that the intense mechanical stresses and strains produced during ball milling might alter the crystal structure of STO, possibly inducing a non-centrosymmetric distortion. This induced strain could hypothetically activate piezoelectric properties in a material that is naturally piezo-inactive. The present study is intended to explore the ability of the ball milling process to instigate mechano-catalytic activity in STO for the degradation of MB dye. The performance obtained *via* ball milling process is compared with that *via* ultrasonication to critically evaluate the potential of ball milling. Further, the effect of various parameters, which influence the overall activity of the catalyst, has also been studied.

2. Experimental section

2.1 Material

STO nanoparticles were purchased from Nanografi Nano Technology, USA. MB dye was used to prepare synthetic polluted water. For mechanocatalysis, the planetary ball mill PM 100 (Retsch) instrument with a milling jar (125 ml volume) and zirconium (Zr) balls as milling balls (of 10 mm diameter size) were utilized.

2.2 Characterisation

STO nanoparticles were characterized by the X-ray diffraction (XRD) technique to confirm their crystallographic orientation using the Rigaku diffractometer which have 9 kW rotating Cu Kα (λ = 1.54 Å) source to record the diffraction pattern. The diffraction pattern (2θ) was obtained within the range of 20° to 80°, employing a step size of 2° min^{-1}. The bonds present in the molecular structure of STO nanoparticles are authenticated by Fourier Transform Infra-Red Spectroscopy (Cary 600 Agilent Technology). Further confirmation of the chemical structure was achieved through Raman spectroscopy, utilizing the Lab RAM HR evolution model by Horiba with a 532 nm wavelength laser. UV-vis spectroscopy was employed to deduce the energy band gap of STO nanoparticles using a UV-visible

spectrophotometer (SHIMADZU-2600). Scanning electron microscopy (SEM) images were captured using the FE-SEM Inspect S50 model to explore the morphology of the catalyst powder. For this purpose, the catalyst powder underwent sonication and was then drop-cast into water, followed by a gold coating to maintain charge neutrality. To determine average particle size distribution, ImageJ software was used to measure the dimensions of particles from FESEM images. Further, elemental colour mapping and EDAX spectrum were obtained to roughly estimate the ratios of different elements present in the catalyst. To delve into the surface chemistry of the catalyst powder, X-ray photoelectron spectroscopy (XPS) was employed, utilizing instrument Thermo Fisher's Nexsa.

2.3 Degradation experiments using ball milling

Prior to each degradation experiment, STO nanoparticles were dispersed in MB dye for 24 hours to establish equilibrium ensuring clear bifurcation between adsorption and catalytic degradation in subsequent analysis. During these adsorption experiments, no other parameters should affect the process, this was ensured by putting efforts to eliminate the external influences. This included conducting the experiments in dark conditions in an aluminium foil-covered beaker to mitigate the impact of light. Additionally, to facilitate proper mixing while minimizing the effect of triboelectricity, a small magnetic bead and a stirring speed of only 200 rpm were employed. Once equilibrium was achieved, the heterogeneous mixture of dye and catalyst was transferred to a ball milling jar for catalysis. The milling process occurred at regular intervals of 15 minutes for up to 1 hour, with aliquots collected and centrifuged at each interval. These dye aliquots were then analyzed by measuring their absorbance using a UV-visible spectrophotometer (SHIMADZU-2600) within the wavelength range of 400–800 nm. The reduction in the absorbance peak of the MB dye was used to quantify the decrease in dye concentration. The absorbance value of dye is taken as its equivalent concentration value according to Beer–Lambert's law, $A = \varepsilon Cl$ (where, "A" is absorbance of the matter, "ε" is molar absorption coefficient and "l" is the optical path length), thus measure of absorbance can define the amount of concentration when ε and l are kept constant.

2.4 Parametric study in ball milling assisted catalysis

To explore the impact of different process variables, a parametric study was conducted. The thorough analysis offered valuable insights into how factors such as rotation speed, number of milling balls, catalyst dosage, and initial dye concentration influence the catalytic reaction. The experimental design ensured that only one parameter was varied at a time while keeping other parameters constant. For instance, the effect of rotation speed during the milling process was examined by conducting experiments at different speeds of 200 rpm, 300 rpm, and 400 rpm. Similarly, degradation experiments were carried out using 5, 10, and 15 milling balls individually to assess the impact of the number of balls. Catalyst loading was investigated by varying the amounts of catalyst to 0.2 g, 0.3 g, and 0.4 g. Additionally, the initial concentrations of dye were varied from 5 ppm, 10 ppm, to 15 ppm. The obtained rate constants for the degradation reaction in each case were plotted against the corresponding parameter and fitted to derive an empirical expression, demonstrating a pragmatic relationship between them.

3. Results & discussions

The purity of STO nanoparticles was confirmed by XRD pattern (Fig. S1†), Raman spectrum (Fig. S2(a)†), FTIR spectrum (Fig. S2(b)†), absorption spectrum and Tauc's plot (Fig. S3(a) and (b)†), SEM images (Fig. S4(a)–(f)†), and XPS spectrum (Fig. S5(a)–(d)†). The detailed characterisation results have been provided in the ESI file.† After confirming phase purity, the STO nanoparticles were subjected to the adsorption phenomenon, and for this STO were initially brought into contact with MB dye for 24 hours to reach equilibrium, ensuring that subsequent ball milling experiments would result in degradation solely through mechano-catalysis. Following this, the mixture of dye and STO nanoparticles was transferred to the milling jar and subjected to catalysis. The variation of concentration of MB dye with time was analyzed according to the simple form of Langmuir–Hinshelwood (LH) model for pseudo first-order reactions, which is given by the equation:

$$\ln\left(\frac{C}{C_o}\right) = -kt \quad (1)$$

where "C_o" is the initial concentration (at 0 min), "C" is final concentration, "k" is rate constant and "t" is time in min.

To determine the rate constant, the natural logarithm of the ratio of initial and final concentrations $\left(\ln\frac{C}{C_o}\right)$ was plotted against time (t).

The residual concentration of MB dye after adsorption–desorption equilibrium is represented by the 0 min plot in the absorbance spectrum, shown in Fig. 1(a) and (b). This is considered as the initial concentration for ball mill experiments. The subsequent decrease in absorbance of MB dye was observed for different aliquots as time proceeded. This is the signature of degradation happening *via* ball milling. By the end of 1 hour, approximately 70% degradation was achieved using 0.3 g STO at 400 rpm using 10 Zr balls. These results are comparable with the results obtained with $BaTiO_3$ in our previous study.[24] Although $BaTiO_3$, being inherently non-centrosymmetric, demonstrated superior efficiency (77% degradation at 300 rpm), the performance of centrosymmetric STO (70% degradation at 400 rpm) is still commendable as this result is a direct consequence of strain-induced polarization. This impressive result underscores the significant influence of the ball milling process in inducing strain within STO, leading to polarization that would not naturally occur in its centrosymmetric structure. Further, the degradation could also be there due to locally induced polarization developed due to strain gradient within STO structure during collision of milling balls. Moreover, for comparison, a batch of experiments was conducted without adding STO nanoparticles while keeping

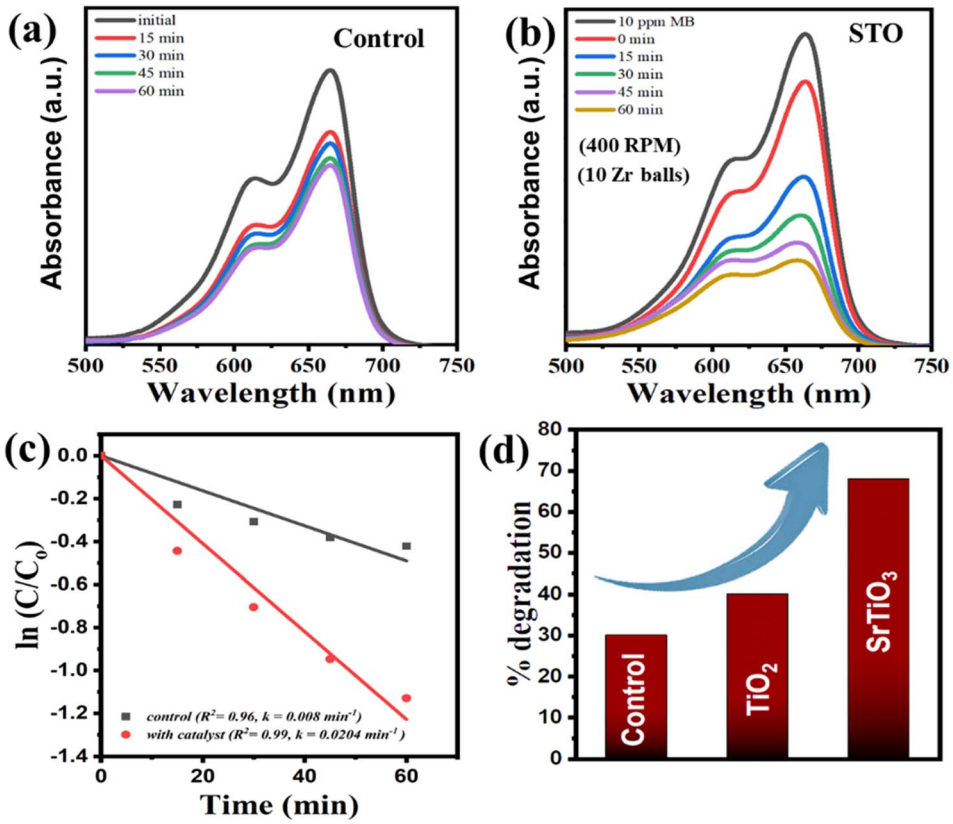

Fig. 1 Absorbance spectrum of MB dye (a) without using catalyst (control), (b) using STO nanoparticles catalyst through ball milling at 400 rpm with 10 balls, (c) plot between $\ln(C/C_o)$ *vs.* time revealing the kinetic rate, (d) comparison of % dye degradation without catalyst (control), TiO_2 and STO as a catalyst at same parameter.

other parameters constant. The absorbance spectrum of MB dye degradation from this control study (without using STO) is shown in Fig. 1(a) and approximately 27% of the dye was degraded in 1 hour. This suggests that self-degradation to some extent can also occur using high energy ball milling catalysis.[36] In the study involving the catalyst, the rate constant was calculated to be 0.0204 min^{-1}, whereas a significantly lower value of 0.008 min^{-1} was obtained for the control study, indicating the considerable influence of our catalyst STO on degradation under ball milling conditions. Furthermore, for comparative purposes, the efficiency of STO was evaluated against known material TiO_2. Under equivalent TiO_2 dosage and similar process parameters, ~40% degradation was achieved (as illustrated in Fig. 1(d)). This comparison highlights the superior performance of STO over TiO_2 in mechanocatalysis applications.

Fig. 2(a)–(e) shows the investigation examined for the effect of the speed of rotating milling machine on catalytic efficacy. A solution containing 30 ml of 10 ppm MB dye, along with 0.3 g of STO nanoparticles and 10 Zr balls, was subjected to milling under various speeds. The decreasing absorbance spectrum of the dye for rotating speeds of 200 rpm, 300 rpm, and 400 rpm is illustrated in Fig. 2(a)–(c) respectively.

It is visually evident that degradation increases with higher speeds. Fig. 2(d) presents the kinetics plots of $\ln(C/C_o)$ *vs.* t for each case. The rate constants, determined as the slope of the fitted line, were 0.0105 min^{-1}, 0.0142 min^{-1}, and 0.0205 min^{-1} for 200 rpm, 300 rpm, and 400 rpm, respectively. This observed increase in degradation rate with rpm can be attributed to the influence of milling speed on the kinetic energy transferred to the milling balls and the material being milled. Elevated milling speeds lead to greater kinetic energy, resulting in more frequent and energetic collisions between the milling balls and the material. Consequently, this enhances grinding efficiency, favouring more effective surface charge separation. Consequently, the generation of ROS species is increased, leading to enhanced degradation. These rate constants (k_{rpm}) were plotted against the speed of the milling machine (rpm), as depicted in Fig. 2(e), and fitted to get an empirical relation represented in eqn (2).

$$k_{rpm} = 0.00005\ \text{rpm} - 0.0003 \quad (2)$$

Further, a series of batch experiments were conducted to investigate the degradation of 30 ml 10 ppm MB dye by 0.3 g of STO nanoparticles at a milling speed of 300 rpm, by varying quantities of milling balls. Fig. 3(a) displays the kinetics plot for 5, 10, and 15 balls. The rate constants, determined from the slope of the fitted line, suggest that an increase in the number of milling balls leads to accelerated degradation kinetics. This phenomenon can be attributed to the greater number of opportunities for energy transfer from the balls to the material,

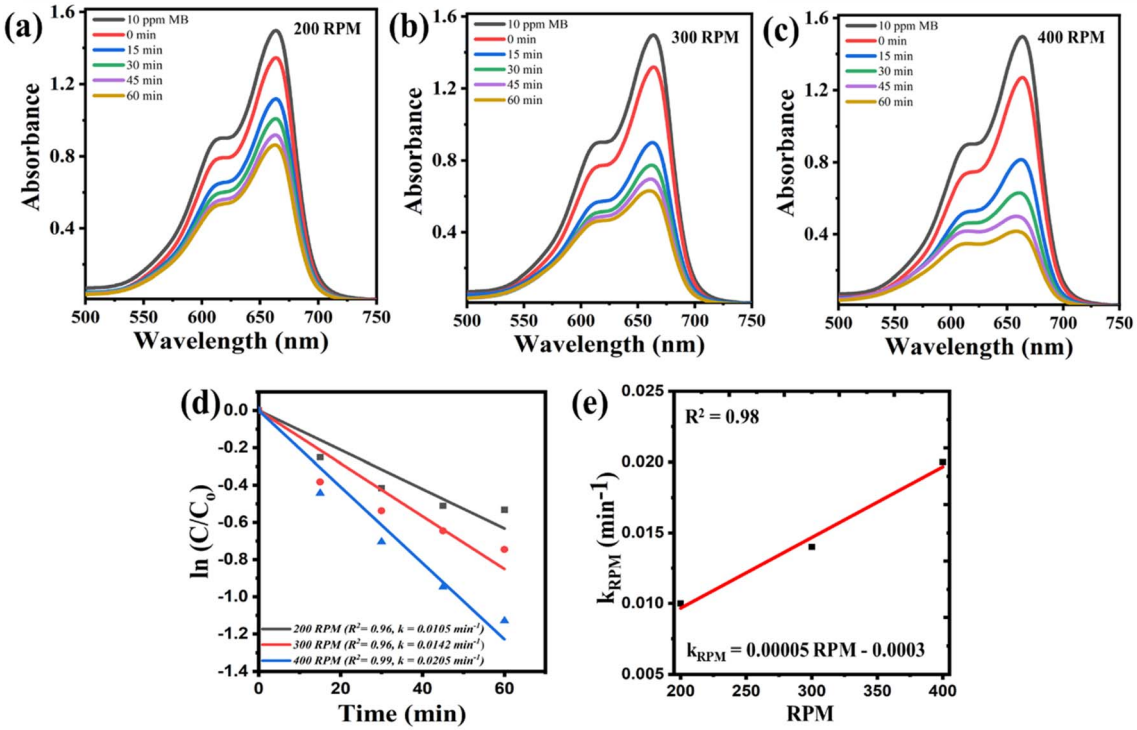

Fig. 2 Absorbance spectra of 10 ppm MB dye with time using 0.3 g STO nanoparticles using 10 milling Zr balls at milling speed (a) 200 rpm (b) 300 rpm and (c) 400 rpm (d) degradation kinetic rate through $\ln(C/C_o)$ *vs.* time plot and (e) variation of rate constant 'k_{rpm}' with rpm.

resulting in increased impact and applied forces. Consequently, this can induce a more effective potential in the STO and facilitate faster milling kinetics. The rate constants (k_B) were then plotted against the quantity of balls (B) and fitted to express the rate constants as a function of the number of balls. The equation derived from this fitting is:

$$k_B = 0.001B + 0.0099 \quad (3)$$

The impact of catalyst dosage on catalytic efficacy was investigated and depicted in Fig. 4(a) and (b). Fig. 4(a) illustrates the kinetics plots of $\ln(C/C_o)$ *vs.* time for experiments conducted with varying dosages of catalysts (0.2 g, 0.3 g, 0.4 g) keeping initial concentration of 10 ppm MB dye, 300 rpm milling speed and using 10 Zr balls. The slope of the fitted line in the plot provided insights into the kinetic behavior of the catalytic reaction as the catalyst loading was systematically increased. These derived rate constants were then plotted against catalyst loading, as depicted in Fig. 4(b). The plot exhibits a consistent rise in the rate constant's value as the catalyst dosage is incrementally elevated. This can be understood as follows: with an increased catalyst dosage, there is a greater number of reactive

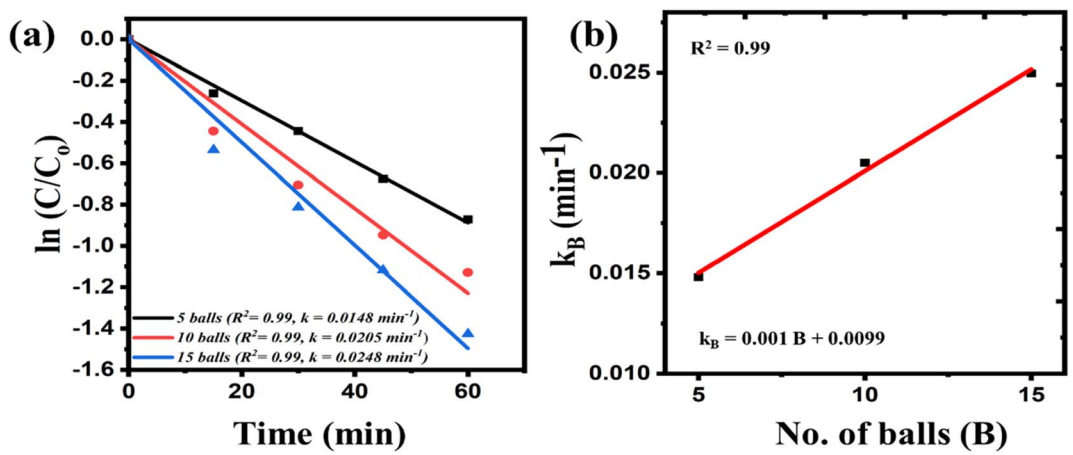

Fig. 3 (a) Degradation kinetics plot showing $\ln(C/C_o)$ *vs.* time revealing the effect of no of balls keeping other parameters constant (0.3 g STO, 10 ppm initial MB dye, milling speed of 300 rpm) and (b) variation of rate constant 'k_B' with no. of balls (B).

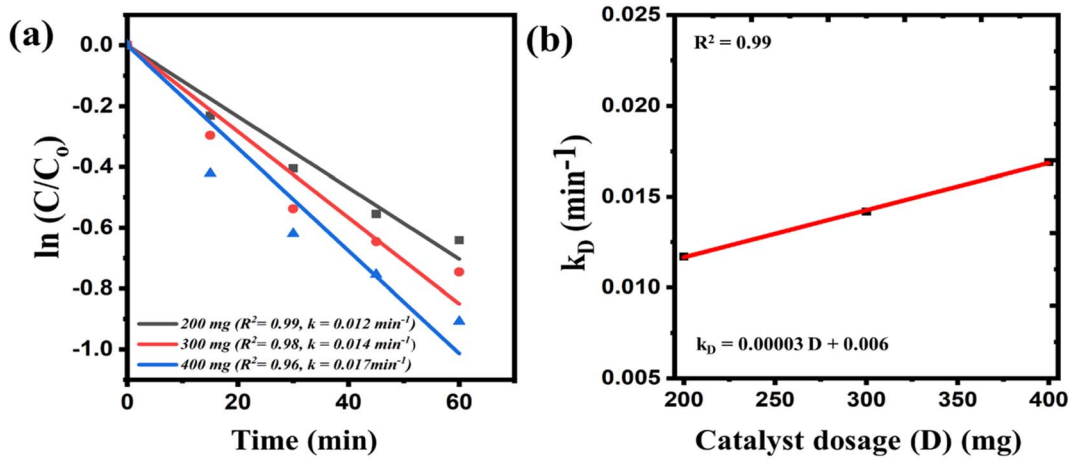

Fig. 4 (a) Degradation kinetics plot of $\ln(C/C_o)$ *vs.* time and (b) variation of rate constant 'k_D' with catalyst dosage (D) by keeping parameters constant (10 ppm initial MB dye, 10 milling balls, milling speed of 300 rpm).

sites available while milling, facilitating the generation of a larger quantity of reactive species, consequently leading to enhanced reaction kinetics. A mathematical equation, fitted to the data points in the plot representing the relationship between the rate constant (k_D) and the elevated amount of catalyst (D) in the solution (Fig. 4(b)), is provided in eqn (4).

$$k_D = 0.00003D + 0.006 \quad (4)$$

Finally, in parametric study, the reaction kinetics was examined by varying the initial concentration of the MB dye aqueous solution from 5 ppm, 10 ppm to 15 ppm (while other parameters remain fixed) and illustrated in Fig. 5(a) and (b). The reaction kinetics to assess this influence is given in Fig. 5(a). The slope of the fitted line, which serves as an indicator of the rate constant changes when a higher concentration of dye was utilized for catalysis. The plot in Fig. 5(b), which was generated to elucidate the pattern of variation of the rate constant concerning the increased initial concentration reveals that the rate constant decreases as the initial concentration of the solution is raised for catalysis. This reduction in the rate constant can be attributed to the augmented quantity of MB dye molecules in the aqueous solution. With higher concentrations of dye, a greater number of reactive species are required to interact with and break down the molecules. The inadequate availability of the necessary reactive species hampers the reaction kinetics and leads to a decline in the rate constant. The expression showing rate constant (k_{IC}) as a function of initial concentration (IC) is given by eqn (5).

$$k_{IC} = -0.0007\mathrm{IC} + 0.02 \quad (5)$$

Generation of reactive species in mechano-catalysis process is the responsible factor for degradation of organic pollutant. Thus, it becomes important to track the most important or dominating reactive species among produced reactive species.

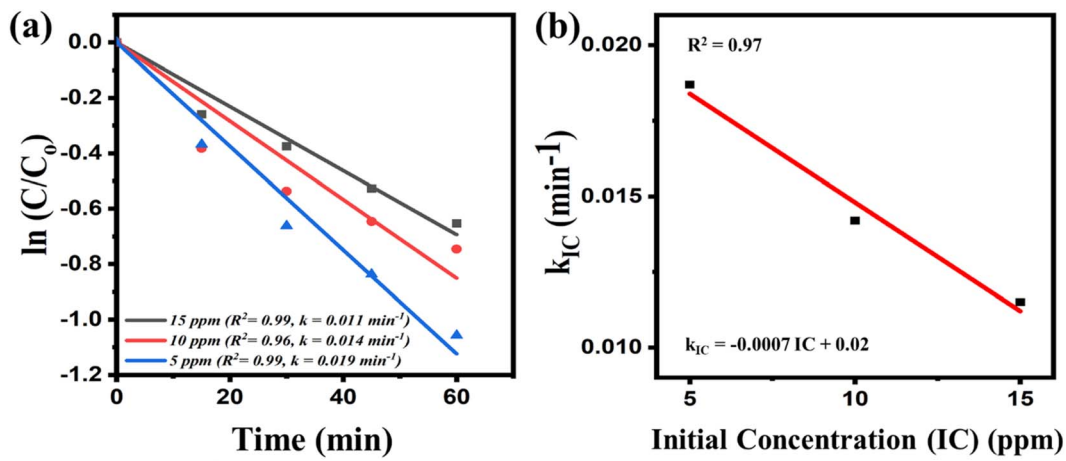

Fig. 5 (a) Degradation kinetics plot of $\ln(C/C_o)$ *vs.* time and (b) variation of rate constant 'k_{IC}' with initial concentration (IC) by keeping other parameters constant (0.3 g STO, 10 milling balls, milling speed of 300 rpm).

Thus, scavenging experiments were performed to investigate the most prominent reactive species responsible for degradation by observing the effectiveness of various scavengers in mitigating the degradation of dyes. Scavengers are compounds or substances that react with reactive intermediates or radicals generated during the degradation process, thereby reducing the degradation rate. We have used 300 μl of 10 mM solutions of isopropyl alcohol (IPA), benzoquinone (BQ), and ethylenediaminetetraacetic acid (EDTA) as scavengers for trapping hydroxyl ($^{\bullet}OH$), superoxide ($^{\bullet}O_2^-$) and hole (h^+), radicals,[37–39] respectively in 30 ml mixture of 10 ppm dye and 0.3 g STO nanoparticles while ball milling at 400 rpm with 10 Zr balls. Fig. 6 illustrates the degradation of dye achieved in the presence of each scavenger using the ball milling technique. The degradation was ~70% when no scavenger has been added. After the addition of scavengers, a decrement in percentage degradation is observed. For IPA, BQ, and EDTA scavengers, the degradation rates were approximately 32%, 20%, and 12%, respectively. It means, h^+, $^{\bullet}O_2^-$, and OH^- all radicals play important roles in degradation because the presence of scavengers of any of these species results in lower degradation. Among all scavengers, EDTA exhibited the lowest degradation rate. Therefore, it can be concluded that holes (h^+) were the most responsible species for degradation by STO using ball milling technique.

Ensuring the stability of the catalyst, post-treatment is crucial to ascertain its efficacy and longevity in catalytic applications. Therefore, following the catalytic treatment, it is imperative to conduct a thorough characterization of the residual catalyst. This process allows for the investigation of any potential alterations in the crystal structure or particle size of the catalytic material. In this regard, the residual STO nanoparticles were typically filtered, subsequently air-dried to eliminate any residual solvents and then analysed using XRD and FESEM techniques.

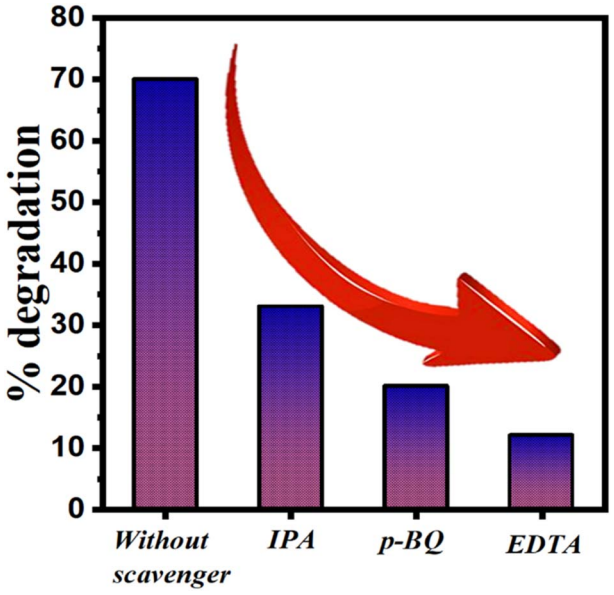

Fig. 6 % degradation in absence and presence of different scavenging species.

Fig. 7(a) illustrates the XRD analysis of STO nanoparticles before and after treatment. The similarity between the XRD peaks of the residual STO nanoparticles and those of the original catalyst confirms the preservation of the crystal structure of the catalyst following the ball milling treatment. A slight shift in the peak position of the (110) plane is observed (as depicted in the zoomed view of Fig. 7(a)), indicating a minor increase in the interplanar distance between the (110) planes. The average crystallite size was determined based on both XRD patterns, revealing a decrease from 47.9 nm to 42.4 nm after the ball milling process. Similar trends were observed for the average particle size measured from the field emission scanning electron microscopy (FESEM) images of STO nanoparticles before and after treatment (depicted in Fig. 7(b) and (c)). The reduction in average particle size from 182 nm to 175 nm was noted. Although this decrease may not be substantial, it is expected given that the STO nanoparticles were subjected to ball milling, a method known for particle size reduction. However, it's worth noting that the reduction is not significant, likely due to the relatively short duration of ball milling, which was conducted for only 1 hour.

The ultrasonication assisted mechanocatalytic performance of STO was assessed through the degradation of MB dye under ultrasonic vibration. A 0.3 g sample of STO was used to degrade 30 ml of 10 ppm MB dye. An ultrasonicator operating at 40 kHz and 140 W was employed to apply ultrasonic vibrations to the heterogeneous solution. To mitigate the effect of thermocatalysis, the ultrasonicator's water was replaced with fresh cold water every 30 min. The experiment was carried out under dark conditions, and samples were collected at regular intervals and subjected to centrifugation for analysis. Fig. 8(a) illustrates the comparison of kinetics, represented by the plot of $\ln(C/C_o)$ *versus* time, for the ultrasonicated assisted mechanocatalytic degradation of dye by STO nanoparticles using an ultrasonicator and degradation using ball milling with an equivalent amount of catalyst. The rate constant obtained for the ultrasonication process is 0.002 min^{-1}, which is notably lower compared to that for ball milling, which stands at 0.0205 min^{-1}. This disparity in rate constants indicates a significantly slower degradation process with ultrasonication.

In Fig. 8(b), the degradation percentage of MB dye by ultrasonication and ball milling, with and without catalyst, is depicted. In the case of ultrasonication, approximately 5% degradation was observed in 1 hour even without catalyst, attributed to the direct interaction of ultrasonic waves with the dye molecules. This degradation increased to 11% when STO nanoparticles were added. Conversely, for ball milling catalysis, the dye exhibited degradation to approximately 27% without catalyst and approximately 70% with the catalyst. These results underscore the superiority of the ball milling method of mechano-catalysis over the ultrasonication process, demonstrating more efficient degradation of the dye under ball milling conditions.

The weakening of MB dye utilizing the ball milling assisted mechano-catalysis process is feasible due to the charge separation induced by the impact force generated by milling balls within a jar. STO nanoparticles flowing with dye gets trapped

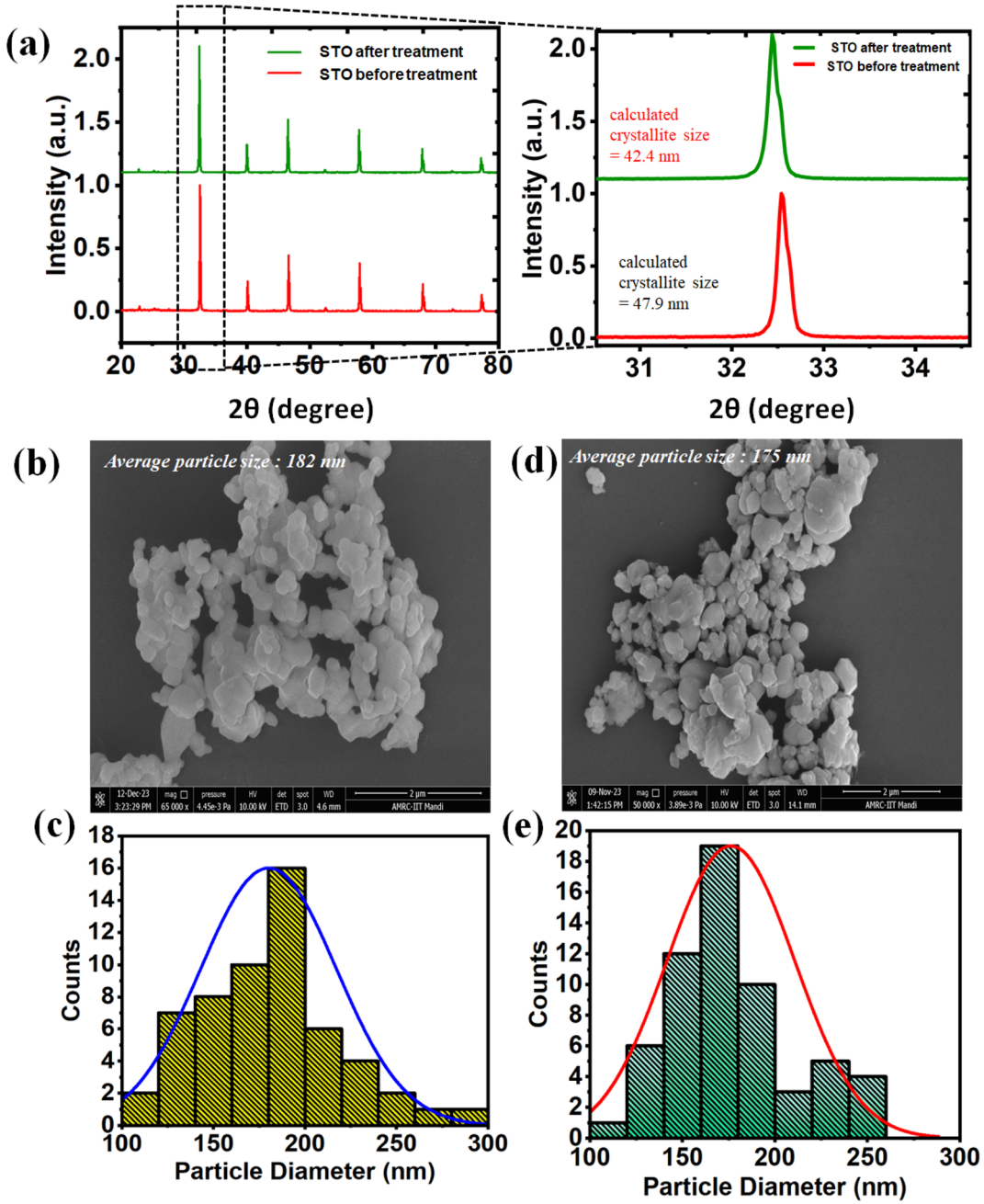

Fig. 7 (a) XRD (with zoomed view) of STO before and after treatment, FESEM images with particle size distribution of STO nanoparticles (b and c) before and (d and e) after catalytic treatment.

between the balls, and the impact force leads to charge separation on the surface of the catalyst. The results of this study demonstrate that a significant amount of degradation was achieved, highlighting the potential of ball milling-assisted catalysis even for centrosymmetric structures. This research is among the first to explore the use of centrosymmetric structured ceramics for dye degradation under the action of mechanical force. While the exact mechanism for the generation of reactive species remains unclear, it is plausible that induced polarization occurs in the STO ceramic during collisions. Additionally, local polarization may be induced due to strain gradients created when the STO ceramic is trapped between two milling balls during the process. Basically, when STO is subjected to mechanical force, the STO prompts a dipole moment to induce polarized positive and negative charges within the material. Consequently, a polarization electric field emerges. Furthermore, this phenomenon concurrently leads to the bending of conduction band (CB) and valence band (VB).[25] This region proves advantageous in facilitating the transfer of charge carriers to the surface, thereby participating in redox reactions. Overall, with high impact force generated during collision positive (h^+) and negative charges (e^-) are generated

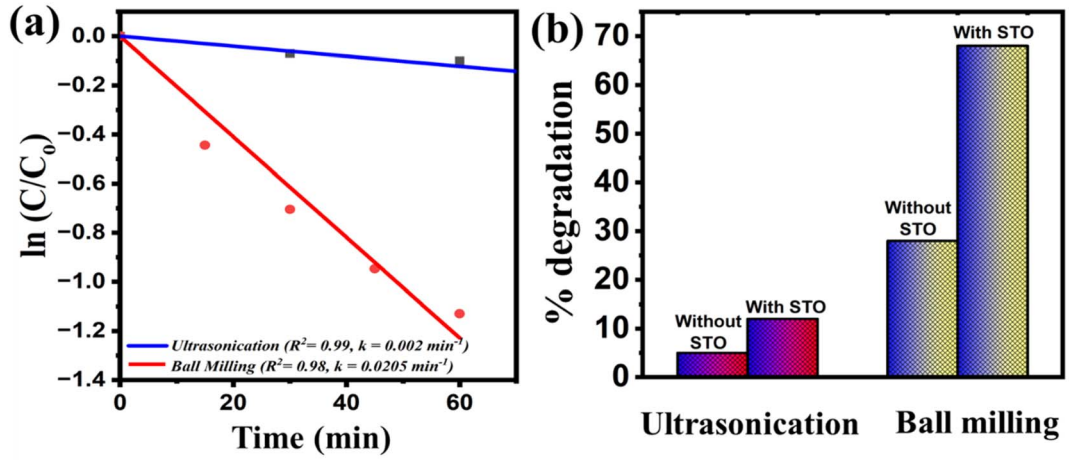

Fig. 8 (a) Kinetic rate in ultrasonication and ball milling assisted catalysis (b) percentage degradation after 1 hour treatment.

which participate in redox reactions, whereby generating reactive species.[40–44] These reactive species disrupt the heterocycle structure of MB dye molecules, leading to their decomposition or weakening. The degradation of MB dye through ball milling assisted mechano-catalysis process can be comprehensively understood through eqn (10)–(13).[24,27]

$$\text{STO} + \text{impact force (through balls)} \rightarrow h^+ + e^- \quad (6)$$

$$O_2 \text{ adsorbed} + e^- \rightarrow {}^{\bullet}O_2^- \quad (7)$$

$$OH^- + h^+ \rightarrow {}^{\bullet}OH \quad (8)$$

$$\text{MB dye} + ({}^{\bullet}OH/{}^{\bullet}O_2^-) \rightarrow \text{dye degradation} \quad (9)$$

In examining the MB dye degradation through ball milling, we can employ the piezocatalysis effect theory, where the induced potential is regarded as a function of the applied force. Fig. 9(a)–(c) shows the schematic representation of top view of mill jar, trajectory of balls in milling jar and schematic representation of production of reactive species while collision. The relationship between the potential induced by strain and the applied force can be represented by eqn (10).[45]

$$V = f_n d_{xy} l_x \varepsilon_{rx} \varepsilon_o \quad (10)$$

In eqn (14), "V" represents the potential induced on the surface of the piezocatalyst due to the applied force. Here, "f_n" signifies the applied normal force in the y-coordinate, "d_{xy}" denotes the piezoelectric coefficient, "l_x" represents the length of STO in the coordinate system, while "ε_{rx}" and "ε_o" stand for the relative permittivity and permittivity of free space, respectively. It's evident that among these factors, "f_n" holds significant influence and can be considered a function of the induced potential. However, in the ball milling-assisted piezocatalysis process, the applied force on the piezocatalyst correlates directly with the ball milling parameters. To enhance comprehension, a sports model was adopted and expressed in eqn (11)–(14).[46,47]

$$f_n = p\pi r^2 \quad (11)$$

$$p = g_p v^{0.4} (\rho/E_e)^{0.2} E_e \quad (12)$$

$$v = \sqrt{(\Omega r_d)^2 + (\Omega - \omega)^2 r_v^2 + 2\Omega(\Omega - \omega) r_d r_v \cos\phi} \quad (13)$$

$$\cos\phi = -\frac{r_v(\Omega - \omega)^2}{r\Omega^2} \quad (14)$$

In the sports model, various assumptions are made, resulting in the trajectory of milling balls being depicted as moving from position (B1) to position (B2), as illustrated in Fig. 9(b). Here, "ϕ" represents the rotation angle of the milling ball, while "Ω" and "ω" denote the angular velocities of the planetary disk and vial, respectively, measured at radii indicated as "r" and "r_d".

Basically, there are two key aspects to dye degradation *via* ball milling catalysis: the nature and type of catalyst used, and the working conditions/parameters of the ball milling. Eqn (10) illustrates the nature of the catalyst, showing that the potential developed in the ceramic, which possesses specific dielectric properties, is driven by the force applied by the milling balls. This force is directly linked to parameters such as the rotation angle of the milling ball and the angular velocities involved in ball milling. These influencing parameters, presented in eqn (11)–(14) from previous literature, can be collectively observed by varying the speed and the milling balls. Through the preceding discussions, it becomes evident that the weakening of MB dye using ball milling is directly linked to the force exerted by the milling balls. Moreover, this applied force can be viewed as a function of both the velocity of the planetary disk and the collision of balls within the jar.

The parametric study using STO in mechano-catalysis *via* ball milling process validate such theory as more effective force can be generated when there is an increase in milling speed while keeping quantity of balls same or increasing the quantity of balls while keeping the speed same. Moreover, increase in speed or balls can also leads to higher degradation of MB dye.

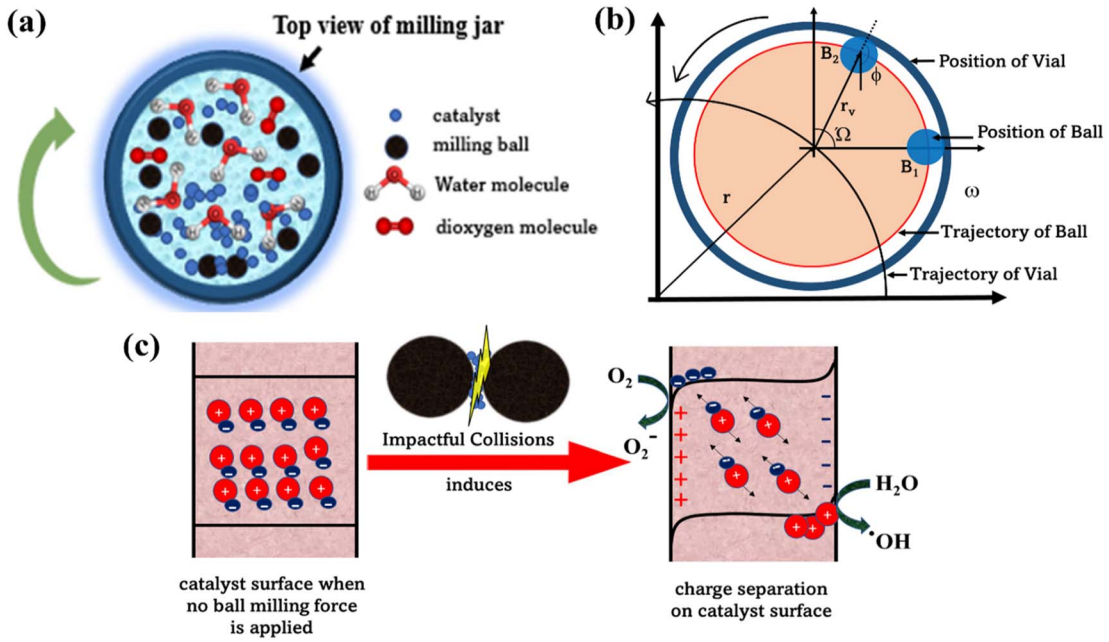

Fig. 9 (a) Top view representation of ball milling jar, (b) trajectory of balls in milling jar, and (c) schematic representation showing production of reactive species when STO gets trapped between two balls during collision.

As in the present study, there is increase in the kinetic rate of degradation of MB dye from 0.0105 min^{-1} to 0.0205 min^{-1} with variation in speed from 200 to 400 rpm, also with increase in the quantity of balls there is increase in the value kinetic rate. Thus, with increase in the value of both parameters of no of balls and speed there is more possibility of higher collisions which creates more reactive species responsible for degradation of MB dye.

Furthermore, there is a possibility of triboelectric effect in degradation of the MB dye.[48] The tribocatalysis process is known for degradation of pollutant by virtue of contact induced surface electrification. STO is a centrosymmetric material thus full mechanism of degradation of MB dye *via* piezocatalysis cannot be justified. However, with centrosymmetric material surface piezoelectricity can produce reactive species when mechanical vibrations are been subjected to them. The charge generated on the surface due to mechanical excitation is also capable of generating reactive species responsible for degradation of dye. Further, tribocatalytic effect can also be a responsible factor for degradation of dye in ball milling assisted mechano-catalytic process.[48] However, it is not possible to differentiate the effect of tribocatalysis and piezocatalysis in mechano-catalysis process utilizing ball milling technique.

4. Conclusions

Traditionally, ball milling is utilized for mechanical grinding of solid materials through milling balls in milling jar. However, in the present study we have utilized ball milling machine for dye degradation application. We demonstrated that the mechano-catalytic activity can be induced by ball milling, even in centrosymmetric STO nanoparticles for the degradation of toxic methylene blue (MB) dye. Various parametric studies were conducted to analyze the impact of different process conditions, including catalyst dosage, initial dye concentration, ball milling speed, and the number of milling balls. The maximum degradation of MB dye (10 ppm) in entire parametric study was found to be ~70% within just 1 hour at a speed of 400 rpm with 10 Zr balls. Furthermore, we compared the ball milling process with the conventional ultrasonication method of STO, which showed only 12% degradation in the same duration (1 hour). The present study explores the superiority of ball milling catalysis, offering precise control over reaction parameters under environmentally friendly conditions.

Data availability

The authors confirm that the data supporting the findings of this study are available within the article and its ESI.†

Conflicts of interest

There are no conflicts to declare.

References

1 R. Ahlunijar, A. F. Wahid, M. A. F. Akmal, C. K. C. Rengganis, S. Karuniawati and H. Kholim, Safety Education through Risk Analysis in the Printing Informal Sector, *J. Saf. Educ.*, 2023, **1**(2), 43–48.
2 J. Jimenez-Paz, J. J. Lozada-Castro, E. Lester, O. Williams, L. Stevens and J. Barraza-Burgos, Solutions to hazardous wastes issues in the leather industry: adsorption of chromium iii and vi from leather industry wastewaters

using activated carbons produced from leather industry solid wastes, *J. Environ. Chem. Eng.*, 2023, **11**(3), 109715.
3 S. Dutta, S. Adhikary, S. Bhattacharya, *et al.*, Contamination of textile dyes in aquatic environment: adverse impacts on aquatic ecosystem and human health, and its management using bioremediation, *J. Environ. Manage.*, 2024, **353**, 120103.
4 T. Akter, A. T. Protity, M. Shaha, M. Al Mamun and A. Hashem, *The impact of textile dyes on the environment, Nanohybrid Materials for Treatment of Textiles Dyes*, Springer, 2023, pp. 401–431.
5 J. Lin, W. Ye, M. Xie, *et al.*, Environmental impacts and remediation of dye-containing wastewater, *Nat. Rev. Earth Environ.*, 2023, **4**(11), 785–803.
6 M. A. Mudassir, S. Kousar, M. Ehsan, *et al.*, Emulsion-derived porous carbon-based materials for energy and environmental applications, *Renewable Sustainable Energy Rev.*, 2023, **185**, 113594.
7 S. Das, L. Cherwoo and R. Singh, Decoding Dye Degradation: Microbial Remediation of Textile Industry Effluents, *Biotechnol. Notes*, 2023, 64–76.
8 D. Rana, T. Matsuura, M. A. Kassim and A. F. Ismail, Reverse osmosis membrane, *Handb. Membr. Sep.*, CRC Press, 2023, pp. 6–32.
9 R. Das, C. D. Vecitis, A. Schulze, *et al.*, Recent advances in nanomaterials for water protection and monitoring, *Chem. Soc. Rev.*, 2017, **46**(22), 6946–7020.
10 M. P. Rayaroth, G. Boczkaj, O. Aubry, U. K. Aravind and C. T. Aravindakumar, Advanced oxidation processes for degradation of water pollutants—ambivalent impact of carbonate species: a review, *Water*, 2023, **15**(8), 1615.
11 C. Porwal, A. Gaur, V. S. Chauhan and R. Vaish, Enhancing Piezocatalytic Dye Degradation through Ball Milling-Induced Polarization in Nano Bismuth Zinc Borate, *Surf. Interfaces*, 2023, 103391.
12 A. Gaur, C. Porwal, D. Singh, V. S. Chauhan and R. Vaish, Facilitating Flexoelectric Effect in BaTiO3 Ceramic for Pollutant Removal Application via Piezocatalysis Process, *Colloids Surf., A*, 2024, 133563.
13 S. Zhao, M. Liu, Y. Zhang, *et al.*, Harvesting mechanical energy for hydrogen generation by piezoelectric metal–organic frameworks, *Mater. Horiz.*, 2022, **9**(7), 1978–1983.
14 P. T. T. Phuong, D.-V. N. Vo, N. P. H. Duy, *et al.*, Piezoelectric catalysis for efficient reduction of CO2 using lead-free ferroelectric particulates, *Nano Energy*, 2022, **95**, 107032.
15 S. Lan, C. Yu, F. Sun, *et al.*, Tuning piezoelectric driven photocatalysis by La-doped magnetic BiFeO3-based multiferroics for water purification, *Nano Energy*, 2022, **93**, 106792.
16 S. Banerjee, S. Bairagi and S. W. Ali, A critical review on lead-free hybrid materials for next generation piezoelectric energy harvesting and conversion, *Ceram. Int.*, 2021, **47**(12), 16402–16421.
17 C. Tong and C. Tong, Emerging materials for energy harvesting, *Introd. to Mater. Adv. Energy Syst.*, 2019, pp. 719–817.
18 Y. Bai, Y. Liu, H. Lv, *et al.*, Processes of electrospun polyvinylidene fluoride-based nanofibers, their piezoelectric properties, and several fantastic applications, *Polymers*, 2022, **14**(20), 4311.
19 P. P. Khirade and A. V. Raut, Perovskite structured materials: synthesis, structure, physical properties and applications, *Recent Adv. Multifunct. Perovskite Mater.*, IntechOpen, 2022.
20 D. Meroni and C. L. Bianchi, Ultrasound waves at the service of photocatalysis: from sonochemical synthesis to ultrasound-assisted and piezo-enhanced photocatalysis, *Curr. Opin. Green Sustainable Chem.*, 2022, **36**, 100639.
21 A. P. Amrute, J. De Bellis, M. Felderhoff and F. Schüth, Mechanochemical synthesis of catalytic materials, *Chem.–Eur. J.*, 2021, **27**(23), 6819–6847.
22 A. Stolle, T. Szuppa, S. E. S. Leonhardt and B. Ondruschka, Ball milling in organic synthesis: solutions and challenges, *Chem. Soc. Rev.*, 2011, **40**(5), 2317–2329.
23 S. Zhou, J. Hao, M. Zhou, X. Qiao and X. Pang, Combination of piezoelectric additives and ball milling for high-efficiency degradation of organic dye in solid state, *Appl. Catal., A*, 2022, **629**, 118406.
24 A. Gaur, V. S. Chauhan and R. Vaish, Planetary ball milling induced piezocatalysis for dye degradation using BaTiO3 ceramics, *Environ. Sci.: Adv.*, 2023, **2**(3), 462–472.
25 X. Liao, H. Xie, B. Liao, S. Hou, Y. Yu and X. Fan, Ball milling induced strong polarization electric fields in Cu3B2O6 crystals for high efficiency piezocatalysis, *Nano Energy*, 2022, **94**, 106890.
26 L. Song, T. Zhang, S. Zhang, J. Wei and E. Chen, Study on performance and mechanism of the ball-milling-driven piezoelectrochemical effect on catalytic oxidation of toluene in the air condition, *ACS Sustain. Chem. Eng.*, 2022, **10**(16), 5129–5137.
27 S. Dubey, A. Gaur, N. Alfryyan, Z. A. Alrowaili, M. S. Al-Buriahi and R. Vaish, Ball Milling based Piezocatalysis using $0.5Ba(Zr_{0.2}Ti_{0.8})O_3$-$0.5(Ba_{0.7}Sr_{0.3})TiO_3$ Ceramics, *Int. J. Appl. Ceram. Technol.*, 2023, 3725–3734.
28 T. P. Yadav, R. M. Yadav and D. P. Singh, Mechanical milling: a top down approach for the synthesis of nanomaterials and nanocomposites, *Nanosci. Nanotechnol.*, 2012, **2**(3), 22–48.
29 B. L. Phoon, C. W. Lai, J. C. Juan, P. Show and W. Chen, A review of synthesis and morphology of SrTiO 3 for energy and other applications, *Int. J. Energy Res.*, 2019, **43**(10), 5151–5174.
30 Z. Kuspanov, A. Umirzakov, A. Serik, A. Baimenov, M. Yeleuov and C. Daulbayev, Multifunctional strontium titanate perovskite-based composite photocatalysts for energy conversion and other applications, *Int. J. Hydrogen Energy*, 2023, 38634–38654.
31 Y. Xu, Y. Liang, Q. He, *et al.*, Review of doping SrTiO3 for photocatalytic applications, *Bull. Mater. Sci.*, 2022, **46**(1), 6.
32 Y. Xin, J. Jiang, K. Huo, T. Hu and P. K. Chu, Bioactive SrTiO3 nanotube arrays: strontium delivery platform on Ti-based osteoporotic bone implants, *ACS Nano*, 2009, **3**(10), 3228–3234.

33 Y. Wang, D. Zhang, C. Wen and Y. Li, Processing and characterization of SrTiO3–TiO2 nanoparticle–nanotube heterostructures on titanium for biomedical applications, *ACS Appl. Mater. Interfaces*, 2015, **7**(29), 16018–16026.
34 Y. Fu, X. Li, C. Sun, *et al.*, pH-triggered SrTiO3: Er nanofibers with optically monitored and controlled drug delivery functionality, *ACS Appl. Mater. Interfaces*, 2015, **7**(45), 25514–25521.
35 Y. Chen, A. Gao, L. Bai, *et al.*, Antibacterial, osteogenic, and angiogenic activities of SrTiO3 nanotubes embedded with Ag2O nanoparticles, *Mater. Sci. Eng., C*, 2017, **75**, 1049–1058.
36 W. Pickhardt, S. Grätz and L. Borchardt, Direct mechanocatalysis: using milling balls as catalysts, *Chem.–Eur. J.*, 2020, **26**(57), 12903–12911.
37 A. Gaur, M. Sharma, V. S. Chauhan and R. Vaish, Visible light photocatalytic activity in BiFeO3 glass-ceramics, *Mater. Chem. Phys.*, 2023, **303**, 127710.
38 A. Gaur, M. Sharma, V. S. Chauhan and R. Vaish, BaTiO 3 crystallized glass-ceramic for water cleaning application via piezocatalysis, *Nano-Struct. Nano-Objects*, 2023, **35**, 101005.
39 C. Porwal, S. Verma, A. Gaur, V. S. Chauhan and R. Vaish, Bi2ZnB2O7–PVDF electrospun composite membrane for waste water treatment utilizing photo-piezocatalysis, *Mater. Sci. Eng., B*, 2023, **298**, 116842.
40 K. Kubota, Y. Pang, A. Miura and H. Ito, Redox reactions of small organic molecules using ball milling and piezoelectric materials, *Science*, 2019, **366**(6472), 1500–1504.
41 T. Seo, K. Kubota and H. Ito, Dual Nickel(II)/Mechanoredox Catalysis: Mechanical-Force-Driven Aryl-Amination Reactions Using Ball Milling and Piezoelectric Materials, *Angew. Chem., Int. Ed.*, 2023, **62**(42), 243–278.
42 Y. He, G. Wang, W. Hu, *et al.*, Piezocatalyzed Decarboxylative Acylation of Quinoxalin-2(1H)-ones Using Ball Milling, *ACS Sustain. Chem. Eng.*, 2023, **11**(3), 910–920.
43 M. M. Amer, R. Hommelsheim, C. Schumacher, D. Kong and C. Bolm, Electro-mechanochemical approach towards the chloro sulfoximidations of allenes under solvent-free conditions in a ball mill, *Faraday Discuss.*, 2022, **241**, 79–90.
44 M. Lucero, D. B. Armitage, X. Yang, *et al.*, Ball Milling-Enabled Fe2.4+ to Fe3+ Redox Reaction in Prussian Blue Materials for Long-Life Aqueous Sodium-Ion Batteries, *ACS Appl. Mater. Interfaces*, 2023, **15**(30), 36366–36372.
45 M. B. Starr and X. Wang, Fundamental analysis of piezocatalysis process on the surfaces of strained piezoelectric materials, *Sci. Rep.*, 2013, **3**(1), 1–8.
46 S.-Y. Lu, Q.-J. Mao, Z. Peng, X.-D. Li and J.-H. Yan, Simulation of ball motion and energy transfer in a planetary ball mill, *Chin. Phys. B*, 2012, **21**(7), 78201.
47 P. P. Chattopadhyay, I. Manna, S. Talapatra and S. K. Pabi, A mathematical analysis of milling mechanics in a planetary ball mill, *Mater. Chem. Phys.*, 2001, **68**(1–3), 85–94.
48 Z. Wang, X. Dong, X.-F. Li, *et al.*, A contact-electro-catalysis process for producing reactive oxygen species by ball milling of triboelectric materials, *Nat. Commun.*, 2024, **15**(1), 757.